Farm-Scale Water Storage in Morocco: Coupling Finite Element Analysis and Parametric Optimization for Rectangular Reinforced Concrete Structural Layouts

Raphaël TREZARIEU[*], Jad SADEK[a], Josephine CARSTENSEN[b]

[*,b] Massachusetts Institute of Technology, Department of Civil and Environmental Engineering
77 Massachusetts Avenue, Cambridge, MA 02139, USA
raphtrez@mit.edu

[a] Setec Travaux Publics et Industriels
42 Quai de la Rapée, 75012 Paris, France
jad.sadek@setec.com

Abstract

Morocco faces increasing water scarcity with an anticipated decline in rainfall. Rising temperatures have resulted in drier and denser soil, causing water to be trapped on the surface and evaporate. One solution is to shift water management from large-scale to farm-scale. Underground water reservoirs allow the catchment of sparse rainfall events and the resultant overland flows before their evaporation. This research develops a methodology to design such prismatic reinforced concrete water reservoirs using a parametric approach in Python coupled with a Finite-Element Analysis (FEA) software. The aim is to offer both low embodied carbon and affordable designs, for an individual farmer to build. The first method section is used to identify a small region of the design space containing the Pareto front before running FEA on a limited set of geometries in the second section.

Keywords: Parametric Optimization, Finite Element Analysis, Embodied Carbon, Python, Water Reservoir Design, Design Space Exploration, Pareto Front, Design Diversity

1. Introduction

Morocco faces increasing water scarcity, with projected rainfall reductions ranging from 20% to 50% across various climate scenarios as underlined in Figure 1. As temperatures increase, the soil becomes drier and denser, causing water to be trapped on the surface and evaporate, or directly infiltrate the ground. Additionally, changing rainfall patterns lead to sparser and more intense events which exacerbate the situation. This decreased water availability poses a significant challenge for agriculture, with only 600m^3 of water per inhabitant already, falling below the scarcity threshold of 1000m^3 per inhabitant [1]. One solution is to shift water management from large-scale to farm-scale. Smaller underground reservoirs would allow the catchment of sparse rainfall events across the country and would allow the catchment of overland flow before its evaporation [2]. Such reservoirs can be built in remote areas to provide local water production sites and complement the water distribution network for enhanced resilience. The scale of reservoirs for individual farmers would be in the order of magnitude of 1000m^3/ha, depending on the low number of extreme rainfall events able to fill the reservoir and the water needs of the type of crop. With water being stored for long periods, no evaporation can be tolerated in opposition to traditional surface-level irrigation reservoirs, and no sunlight can reach the water to avoid eutrophication. Underground Reinforced Concrete (RC) reservoirs are an option to protect the water but they can

be material intensive with large quantities of concrete and steel accounting for a high cost and embodied carbon footprint, further impacting climate change. Using the reservoir's volume as an input parameter, the overall goal of this work is to automate the design of such structures for the farmers in Morocco, while reducing the embodied carbon.
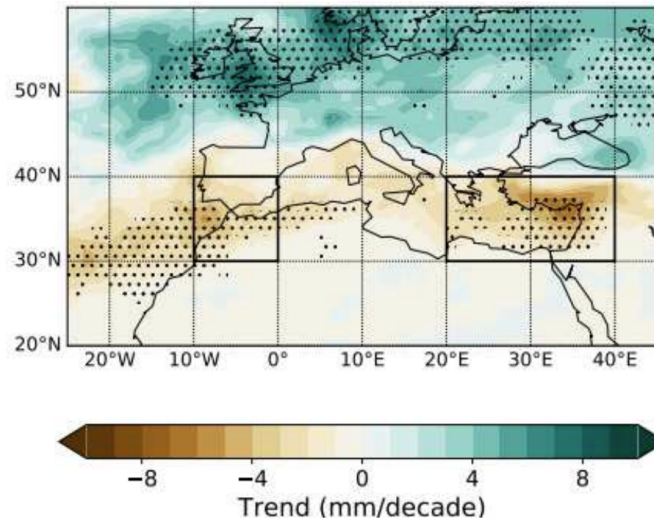

Figure 1: Mediterranean precipitation under RCP8.5 (2071–2100 minus 1976–2005), Tuel et al. [3] ©American Meteorological Society. Used with permission.

The application of structural optimization methodologies to RC water reservoirs has been historically limited, with the exception of one notable approach that managed to reduce the cost of an RC reservoir by using a commercial software implementing a genetic algorithm (GA) coupled with Finite Element Analysis (FEA) [4]. The distinction of the structural elements and the use of FEA was successful and is shared in this paper. However, the black box optimization does not allow the user to control the design of the structural elements individually, has a prolonged computational time, and optimizes only one objective.

The parametric FEA optimization developed in this work allows the designer to integrate performance and diversity in the design space exploration, aligning with the principles discussed by Danhaive and Mueller [5] and Mueller and Ochsendorf [6]. By creating a design hierarchy from the slabs to the beams, walls, and columns, the designer is exposed to a range of diverse design variants. Her preferences are thus injected all along the design process should it be for environmental, aesthetical, or economical decisions. Recent developments tend to go further in the diversity search to escape regular, rectilinear geometries [7]. However, in certain scenarios such as the design of underground reservoirs, a very regular structure is advantageous. Rectangular shapes are easier, and more affordable to build and coat [4]. While keeping rectangular prismatic geometries, diversity in the designs is important to allow for construction flexibility. It can be difficult to predict all the on-site constraints, so diversity allows the selection of slightly less optimal solutions that will be more constructible.

The integration of multi-objective optimization (MOO) considering both embodied carbon and cost in structural design is a rare occurrence as many studies approximate them through weight or material volume minimization [6]. The embodied carbon and the cost of the structure are related to the material volume but are not always proportional for multi-material structures [8]. Surprisingly, despite the prevalence of FEA in structural design, there exists a notable gap in the literature concerning the coupling of parametric optimization and FEA. Parametric modeling has been extensively coupled to optimization

algorithms [9], but this approach varies from the parametric optimization as defined here: the generation of all possible geometries based on the combinations of design variables under given ranges, their design to the construction codes through analytical relations and load approximations, and their graphic post-processing.

More broadly, the design method developed here is the parametric FEA optimization of RC reservoirs with prismatic elements and a rectangular base. The design process is separated in two code sections: the first section designs the local structural elements to the Eurocodes based on load approximations and allows the fast carbon-cost evaluation of a wide range of design variants. Then, the second section combines the subset of selected structural elements together into entire reservoir variants that are all evaluated through FEA. The internal forces are collected considering hyperstatic effects and load envelopes and used to evaluate the reinforcement ratios with better precision, leading to a final Pareto front of low-carbon and -cost reservoir designs.

In section 2., the methodology is described with the design of the local structural elements, the connection of the selected preliminary designs to the FEA software, and the recombination in a carbon-cost graph of the entire reservoir. In section 3., the results are presented with the comparison of the optimal geometries found with the preliminary stress approximations to the geometries found with the additional FEA, and highlight the embodied carbon and cost reductions compared to a baseline design.

2. Methodology

Local design variables are defined for every local structural element such as beams, columns, slabs, and walls. The design variables are combined into structural element variants that are designed to the Eurocodes before being plotted on an embodied carbon-cost graph. It is then possible to manually select any group of elements on the graph, for example on the Pareto front. The slabs are selected first as they influence the loads on the beams that are chosen second before the columns and walls in parallel. The columns and walls are designed with uniaxial bending interaction diagrams.

The selection and thus initial design process is shown in Figure 3, where a small set of slabs, beam, columns, and walls has been selected by the designer in the cyan circles. The selected reservoir combinations are injected into Pythagore, an FEA software (developed by Setec TPI), and controlled using Python through its API. The maximum moments are collected and used to evaluate the reinforcement ratios a second time for the slabs and beams and are also used with the maximum axial forces to filter the columns and walls designs through the interaction diagrams. Finally, the entire reservoirs are plotted on a single carbon-cost graph.

2.1. Example of Local Structural Element Design: Beams

The first code section handles the design of the local structural elements. For example, a beam is defined by its span and the loads it is subjected to. An optimal combination of concrete quality, height, and width, based on cost and embodied carbon is desired. For a given beam, its depth h, width b, and concrete strength f_{ck} are defined as design variables. h spans between [0.2;1.1]m with a step of 0.05m, b spans between [0.3;1.1]m with a step of 0.05m, and f_{ck} spans between [20, 25, 30, 35, 40, 45, 50, 60, 80] MPa corresponding to the catalog concrete strengths as described in table 1. The associated embodied carbon values are based on French Environmental and Health Data Sheets (FDES) obtained on BETie [10] for XC1 CEM IIA-S concrete under the methodology described by De Wolf et al. [11]. The associated cost values are an approximation of the material prices in Morocco and have to be taken with precautions. They correspond to the material price only, without accounting for labor, and are aligned on an 850 DH/m^3 baseline cost of the C20/B25 concrete adding 50 DH/m^3 for every 5 MPa
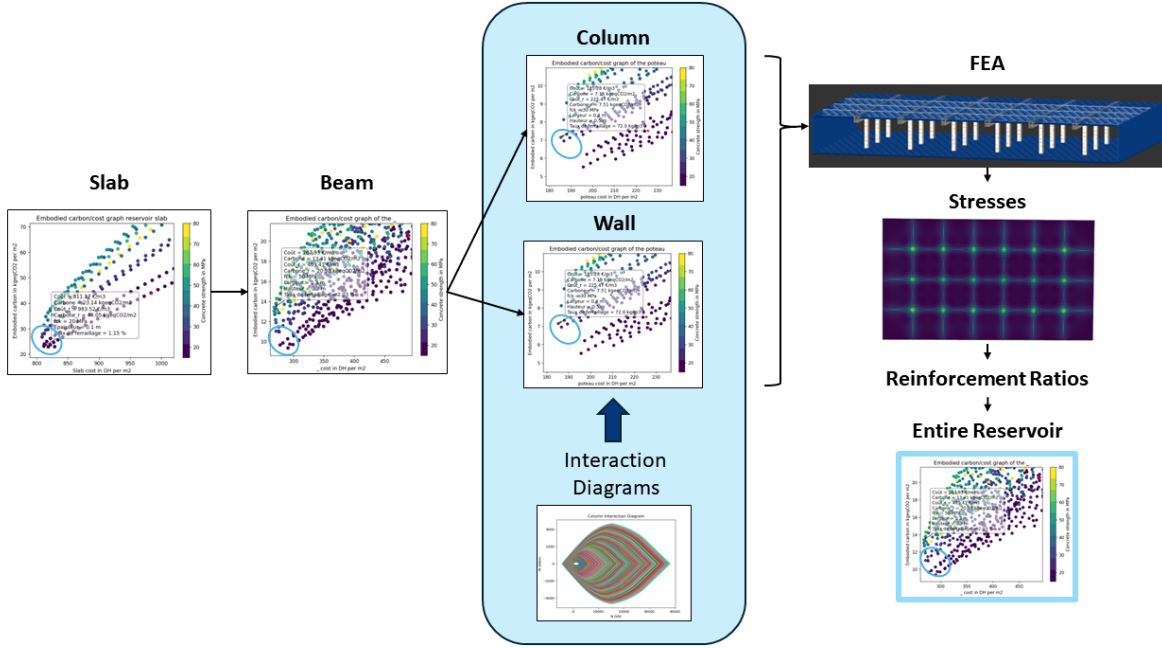
Figure 2: Flowchart of the complete python-FEA code.

increase. The high variability of prices between and inside countries lead to the choice of this simple cost model, rendering the absolute cost values less meaningful. The values that this paper refers to are always the relative cost and carbon reductions compared to a baseline. If precise absolute estimations were required, their calculations would be possible by updating the cost vector. The embodied carbon of the steel rebars is based on an Environmental Product Declaration by ArcelorMittal Europe at 821 kgCO$_2$eq/tonne, with a cost of 13 DH/m^3.

Table 1: Embodied carbon and cost for different strength values of XC1 CEM IIA-S concrete.

Concrete Strength f_{ck} (MPa)	20	25	30	35	40	45	50	60	80
Embodied Carbon (kgCO$_2$eq/m^3)	198	198	212	249	284	300	316	318	342
Cost (DH/m^3)	850	900	950	1000	1050	1100	1150	1250	1450

One combination of the design variables corresponds to one actual beam design. The reinforcement ratio of each design is calculated to the Eurocodes, as described below. First, the section of the flexural steel can be evaluated by solving the system of two equilibrium equations of a beam in simple bending:

$$\begin{cases} 0 = N_{cu} - N_{st} \\ M_{uls} = N_{cu} \cdot z \end{cases} \tag{1}$$

With N_{cu} the ultimate compressive strength in concrete, N_{st} the ultimate tension stress in steel, M_u the ultimate bending moment, and the moment arm z as showned on figure 3.

The centroid of the steel is located at a distance d, known as the effective depth, from the top fiber. The strain diagram is planar across the section height and is characterized by the strain ε_c of the top fiber (compressed concrete) and the strain ε_{st} of the tension steel. The strain is zero at the neutral axis that separates compressed concrete and tensioned concrete. The height of the compressed concrete is de-

noted as αd with $\alpha = \frac{\varepsilon_c}{\varepsilon_c + \varepsilon_{st}}$. The tensioned concrete, located below the neutral axis, is neglected. The stress diagram acting on the compressed concrete is directly derived from the strain diagram by applying the parabola-rectangle law. In simple bending, this diagram can be replaced by a rectangular diagram with a height of $0.8\alpha d$. The compressed concrete area with width b and height $0.8\alpha d$ is subjected to a uniform stress equal to f_{cd}. The resultant compression stress is given by: $N_c = b \cdot 0.8\alpha d f_{cd}$, at a distance of $0.4\alpha d$ from the top fiber. The steel rebars account for a steel section A_s, subjected to a deformation ε_{st} associated to a constraint σ_{st} following the bilinear stress-strain diagram of steel, $N_{st} = A_s \cdot \sigma_{st}(\varepsilon_{st})$ at a height d of the top fiber.
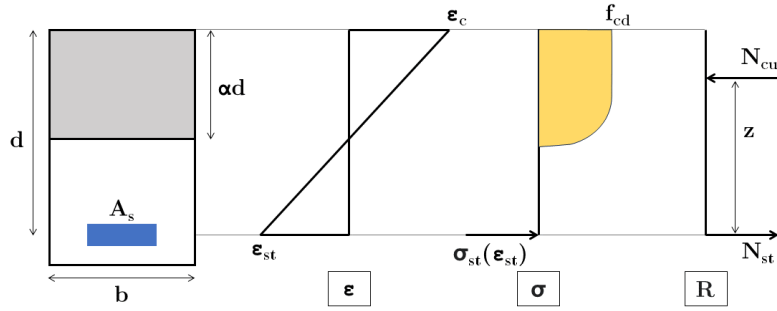

Figure 3: From left to right - The beam section is defined left with the section of steel A_s in blue, the section of compressed concrete in grey of height αd, and d the distance between the centroid of the steel section and the top of the beam. Then, the planar strain diagram across the section height is characterized by the strain ε_c of the top fiber (compressed concrete) and the strain ε_{st} of the tension steel. Third from the left is the associated stress diagram, derived from the strain diagram by applying the parabola-rectangle law. Right displays the resultant efforts in the beam with the compression in concrete N_{cu}, and the tension in the steel N_{st} separated by the moment arm z.

The moment arm z corresponds to the distance between the resultant compression strength in concrete and the resultant tension stress in steel, $z = d - 0.4\alpha d$.

$$z = (1 - 0.4\alpha)d \tag{2}$$

So the second equilibrium equation can be written $M_{uls} = b \cdot 0.8\alpha d f_{cd} \cdot (1 - 0.4\alpha)d$. Regrouping the known quantities, we define the reduced moment μ as:

$$\mu = \frac{M_{uls}}{f_{cd} \cdot b \cdot d^2} = 0.8\alpha(1 - 0.4\alpha) \tag{3}$$

With $f_{cd} = \frac{f_{ck}}{\gamma_c}$, the reduced compressive strength of concrete, and $\gamma_c = 1.5$ the security coefficient for concrete. Thus the solution for the concrete section in compression α:

$$\alpha = 1.25 \cdot \left(1 - \sqrt{1 - 2 \cdot \mu}\right) \tag{4}$$

Knowing the value of μ, α can be found and thus z. The section of steel can be found using the first equilibrium equation inside the second:

$$A_s = \frac{M_{uls}}{z \cdot \sigma_{st}(\varepsilon_{st}(\mu))} \tag{5}$$

Now we specify the expression of M_u. For every beam, the loads at the ultimate limit state are evaluated:

$$q_{\text{uls}} = \psi_G \cdot \left(b \cdot h \cdot \rho_c + \text{slw} \cdot (G + G') \right) + \psi_Q \cdot (\text{slw} \cdot Q) \tag{6}$$

With $\rho_c = 25 kN/m3$ the concrete density, slw the width of the supported slab in m, G the dead load of the supported slab in kN/m², G' the superstructure loads in kN/m², Q the live loads in kN/m², $\psi_G = 1.35$ the load factor of the dead loads, and $\psi_Q = 1.5$ the load factor of the live loads. Then the maximum bending moment is evaluated at mid-span:

$$M_{uls} = \frac{q_{\text{uls}} \cdot \text{L}^2}{8} \tag{7}$$

With L the span of the beam. Then, the stress expression without the tilted branch of the stress-strain diagram is:

$$\sigma_{st}(\varepsilon_{st}) = \begin{cases} \varepsilon_{st} \cdot E_s, & \text{if } \varepsilon_{st} < \frac{f_{yd}}{E_s} \\ f_{yd}, & \text{if } \varepsilon_s \geq \frac{f_{yd}}{E_s} \end{cases} \tag{8}$$

Or considering the tilted branch of the stress-strain diagram (by default):

$$\sigma_{st}(\varepsilon_{st}) = \begin{cases} \varepsilon_{st} \cdot E_s, & \text{if } \varepsilon_{st} < \frac{f_{yd}}{E_s} \\ f_{yd} + (k - 1) \cdot \frac{f_{yd}}{\varepsilon_{uk} - \frac{f_{yd}}{E_s}} \cdot (\varepsilon_{st} - \frac{f_{yd}}{E_s}), & \text{if } \varepsilon_{st} \geq \frac{f_{yd}}{E_s} \end{cases} \tag{9}$$

With $E_s = 200$ GPa the elasticity modulus of steel, $\varepsilon_{uk} = 5\%$ the elongation of steel at break, $f_{yd} = \frac{f_{yk}}{\gamma_s}$, the reduced yield strength of steel ($f_{yk} = 500$ MPa), and $\gamma_c = 1.15$ the security coefficient for steel, and $k = 1.08$. The strain ε_{st} is written:

$$\varepsilon_{st}(\mu) = \begin{cases} \varepsilon_{ud}, & \text{if } \mu < 0.056 \quad \text{(pivot A, steel failure)} \\ \frac{1-\alpha}{\alpha} \cdot \varepsilon_{cu2}, & \text{if } \mu \geq 0.056 \quad \text{(pivot B, concrete failure)} \end{cases} \tag{10}$$

With $\varepsilon_{ud} = 0.9\varepsilon_{uk} = 4.5\%$ the elongation at break for steel, and $\varepsilon_{cu2} = 3.5\%o$ the ultimate strain of concrete. Finally, the reinforcement ratio (in %) can be evaluated:

$$\text{reinforcement ratio} = \frac{A_s}{bh} \tag{11}$$

2.2. Finite Element Analysis

The second code section handles the FEA of the entire reservoir variants. The hierarchy of design from the slabs to the beams, walls, and columns imposes that when a subset of solution is selected from the Pareto front of the carbon-cost graph of the columns, each column solution corresponds to a unique combination of structural elements corresponding to an entire reservoir. Those reservoirs are then linked as inputs of the FEA. The slabs and walls are modeled using 2D elements and the beams and columns are modeled using 1D elements. The mesh size is about 0.3m resulting in 3920 elements.

The integration of the parametric design approach and FEA herein, allows several load combinations to be included as design considerations. This includes complex load combinations such as "checkers loading" highlighted in Figure 4, or different water levels that cannot be evaluated by simpler python scripts. It also takes into account the hyperstatic effects in the structure. However, the computation time is significantly higher with about 20s per model (of which 13s are spent on load combination

and determining the worst-case loads). Finite element analyses of all reservoir variants corresponding to the structural elements combinations would not hence require significant computational resources, motivating the need to carry out the herein-suggested initial reduction of the design space to only a handful of design variants.
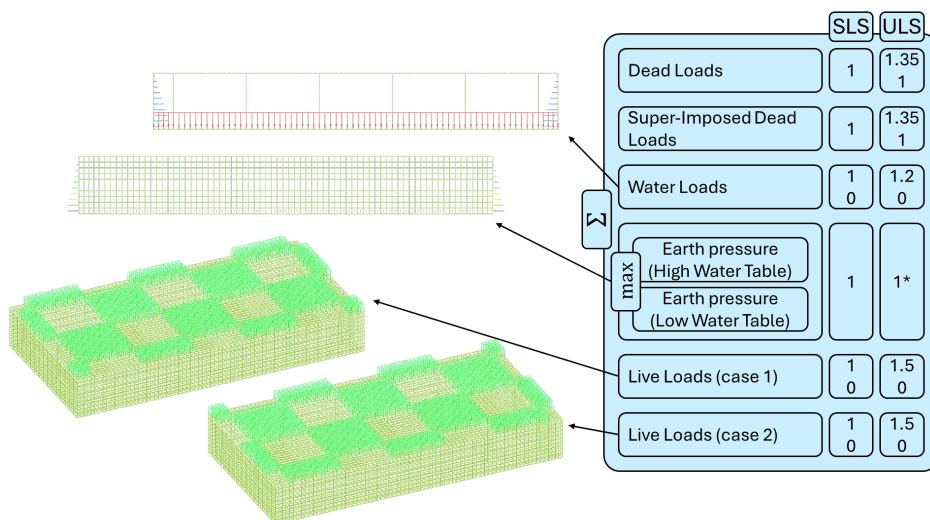

Figure 4: Load cases and upper and lower combination coefficients used in ultimate limit state (ULS), and service limit state (SLS).

3. Results

For the case study examined in this paper, the reference geometry is a square-based reservoir defined by global parameters shown in Figure 5 with the column grid dimensions $l_x = 6$m, and $l_y = 6$m, the number of grid columns $N_x = 3$ and grid rows $N_y = 3$. The height of the reservoir is $h = 4$m. Within the current paper, these global variables are fixed. Furthermore, the reference geometry is made of C20/25 concrete, with a slab thickness of 0.3m, beam width of 0.5m, beam height of 0.85m, wall thickness of 0.3m and square columns of side 0.5m.
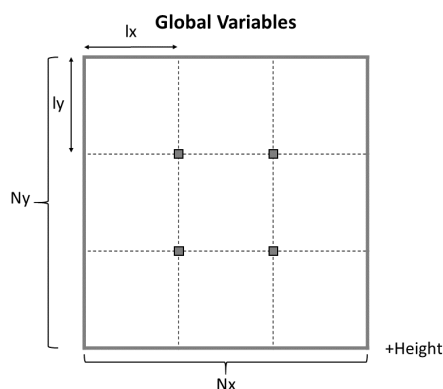

Figure 5: Global parameters definitions in the plan view of the reservoir.

3.1. Beam Carbon-Cost Graph

Figure 6 shows the several thousand beam variants designed in accordance with the Eurocodes on an embodied carbon-cost graph. This graph is one of the four local structural elements graphs returned at the end of the first code section. Every graph highlights a Pareto front of low-carbon and -cost solutions, where every point is one structural element variant. For the herein considered case study, the parametric optimization method developed here leads to an embodied carbon reduction of 65.5% and a cost reduction of 33.9% compared to the reference geometry, with a concrete strength for the beam of $f_{ck,beam} = 35$MPa, a beam width $b_{beam} = 0.3$m, and height $h_{beam} = 0.25$m, a reinforcement ratio of 2.07%, and a slab thickness of 0.1m, with a concrete strength of $f_{ck,slab} = 20$MPa.
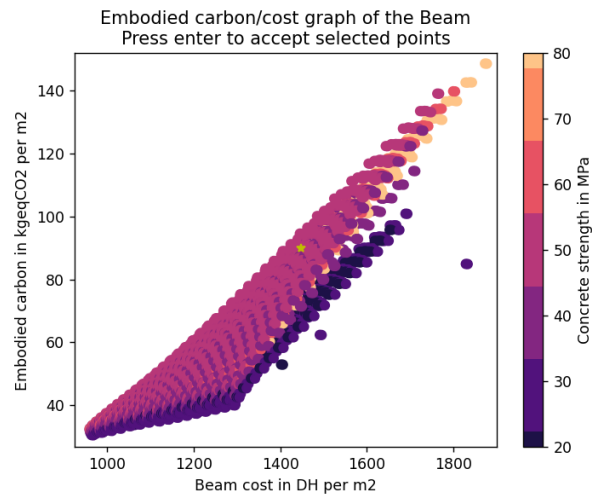

Figure 6: Embodied carbon-cost graph of a representative beam of the system summed to the reductions of the slab. The reference design is indicated by a yellow star.

3.2. Entire Reservoir Carbon-Cost Graph after FEA

At the end of the optimization process, a single carbon-cost graph is returned where each point represents an entire reservoir. The parametric optimization method developed here leads to an embodied carbon reduction of 64.6% and a cost reduction of 38.2% compared to the reference geometry, with a concrete strength for the beam of $f_{ck,beam} = 40$MPa, a beam width $b_{beam} = 0.3$m, and height $h_{beam} = 0.25$m, and a slab thickness of 0.1m, with a concrete strength of $f_{ck,slab} = 20$MPa, column widths $b_{col} = 0.3$m and $h_{col} = 0.4$m in $f_{ck,col} = 20$MPa and a reinforcement ratio of 80 kg/m^3. The reduction values found after FEA are very close to the Python approximations with a relative difference of 3.6% for the cost and 6.8% for the embodied carbon, which supports the approximations and pre-design ran in the first section. The entire code took 10 minutes and 36s to run and obtain the 26 reservoirs presented in Figure 7, each modeled with 3920 finite elements.

4. Conclusion

This paper has explored the optimization of water storage reservoirs in Morocco. In order to exploit the power and precision that an FEA model provides in evaluating forces and stresses, while exploring a large number of solutions, two calculation sections were introduced. The first, relying on a simplified analytical force evaluation, was used to pre-select the candidates that were to be run in the second, relying on FEA software. As most of the calculation time of the FEA pipeline is spent on load combination,
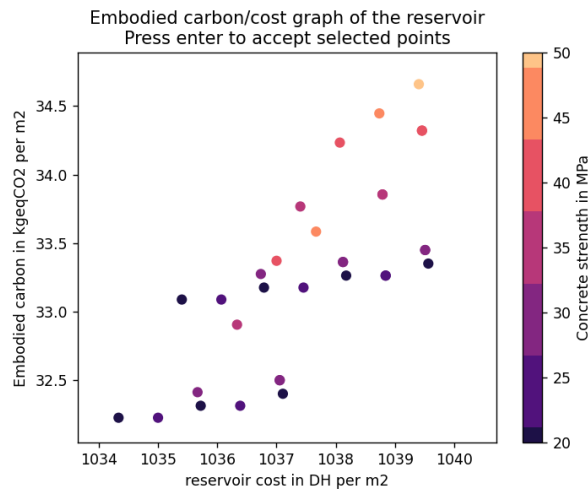
Figure 7: Carbon-cost graph of the entire reservoirs, defined by the previously selected local structural elements, with actualized stresses through FEA.

one way of hastening this pipeline would be to pre-identify the active constraint. In this context, this means to only calculate the load combinations that are known to result in the harshest design criteria. Although identifying those combinations is possible for the geometry at hand, this quickly becomes harder to execute for more irregular shapes.

Finally, the method could be applied to aspects that touch the entire reservoir, as opposed to the structural elements only. For example, the shape of the reservoir has a big impact on its embodied carbon and cost, and making the reservoir deeper to get closer to a cube would reduce the surface of the slabs that are the primary source of embodied carbon and costs, and reduce the overall surface needed to enclose the constant volume. However, a deeper reservoir would imply higher water pressures thus a thicker wall and the method would help find an economical design. Furthermore, the method could solve the column layout optimization problem for the reservoir, and find an equilibrium point between many small columns or a few large columns, while handling their positions and patterns.

Comparing the optimal element solutions to a baseline geometry shows that the method developed in this paper can quickly achieve reductions in both embodied carbon and cost while implementing the designer's preferences through the process. This approach would help individual farmers in Morocco afford reservoirs that are constructible, and reinforce the resilience of the water management system, especially in dry remote regions.

References

[1] A. Tuel, "Precipitation variability and change over Morocco and the Mediterranean," eng, Accepted: 2021-01-05T23:14:29Z, Thesis, Massachusetts Institute of Technology, 2020. [Online]. Available: `https://dspace.mit.edu/handle/1721.1/129036` (visited on 11/02/2023).

[2] A. Vasseur Bendel, "Farm-scale Water Management in Adaptation to Climate Change in Morocco," en, Accepted: 2023-08-23T16:17:43Z, Thesis, Massachusetts Institute of Technology, Jun. 2023. [Online]. Available: `https://dspace.mit.edu/handle/1721.1/151901` (visited on 11/02/2023).

[3] A. Tuel and E. a. B. Eltahir, "Why Is the Mediterranean a Climate Change Hot Spot?" EN, *Journal of Climate*, vol. 33, no. 14, pp. 5829–5843, Jul. 2020, Publisher: American Meteorological Society Section: Journal of Climate, ISSN: 0894-8755, 1520-0442. DOI: `10.1175/JCLI-D-19-0910.1`. [Online]. Available: `https://journals.ametsoc.org/view/journals/clim/33/14/JCLI-D-19-0910.1.xml` (visited on 04/11/2024).

[4] A. Stanton and A. A. Javadi, "An automated approach for an optimised least cost solution of reinforced concrete reservoirs using site parameters," *Engineering Structures*, vol. 60, pp. 32–40, Feb. 2014, ISSN: 0141-0296. DOI: `10.1016/j.engstruct.2013.12.020`. [Online]. Available: `https://www.sciencedirect.com/science/article/pii/S014102961300607X` (visited on 04/13/2024).

[5] R. Danhaive and C. T. Mueller, "Design subspace learning: Structural design space exploration using performance-conditioned generative modeling," *Automation in Construction*, vol. 127, p. 103 664, Jul. 2021, ISSN: 0926-5805. DOI: `10.1016/j.autcon.2021.103664`. [Online]. Available: `https://www.sciencedirect.com/science/article/pii/S0926580521001151` (visited on 04/13/2024).

[6] C. T. Mueller and J. A. Ochsendorf, "Combining structural performance and designer preferences in evolutionary design space exploration," *Automation in Construction*, vol. 52, pp. 70–82, Apr. 2015, ISSN: 0926-5805. DOI: `10.1016/j.autcon.2015.02.011`. [Online]. Available: `https://www.sciencedirect.com/science/article/pii/S0926580515000308` (visited on 04/13/2024).

[7] N. C. Brown and C. T. Mueller, "Design for structural and energy performance of long span buildings using geometric multi-objective optimization," *Energy and Buildings*, vol. 127, pp. 748–761, Sep. 2016, ISSN: 0378-7788. DOI: `10.1016/j.enbuild.2016.05.090`. [Online]. Available: `https://www.sciencedirect.com/science/article/pii/S0378778816304790` (visited on 04/12/2024).

[8] E. Ching and J. V. Carstensen, "Truss topology optimization of timber–steel structures for reduced embodied carbon design," en, *Engineering Structures*, vol. 252, p. 113 540, Feb. 2022, ISSN: 0141-0296. DOI: `10.1016/j.engstruct.2021.113540`. [Online]. Available: `https://www.sciencedirect.com/science/article/pii/S0141029621016345` (visited on 06/05/2023).

[9] R. A. Danhaive and C. T. Mueller, "Combining parametric modeling and interactive optimization for high-performance and creative structural design," *Proceedings of IASS Annual Symposia*, vol. 2015, no. 20, pp. 1–11, Aug. 2015.

[10] *BETie - Présentation*. [Online]. Available: `http://ns381308.ovh.net/ecobilan/presentation.html` (visited on 04/15/2024).

[11] C. De Wolf, F. Pomponi, and A. Moncaster, "Measuring embodied carbon dioxide equivalent of buildings: A review and critique of current industry practice," *Energy and Buildings*, vol. 140, pp. 68–80, Apr. 2017, ISSN: 0378-7788. DOI: `10.1016/j.enbuild.2017.01.075`. [Online]. Available: `https://www.sciencedirect.com/science/article/pii/S0378778817302815` (visited on 04/15/2024).